SUPPLEMENTAL FIGURES

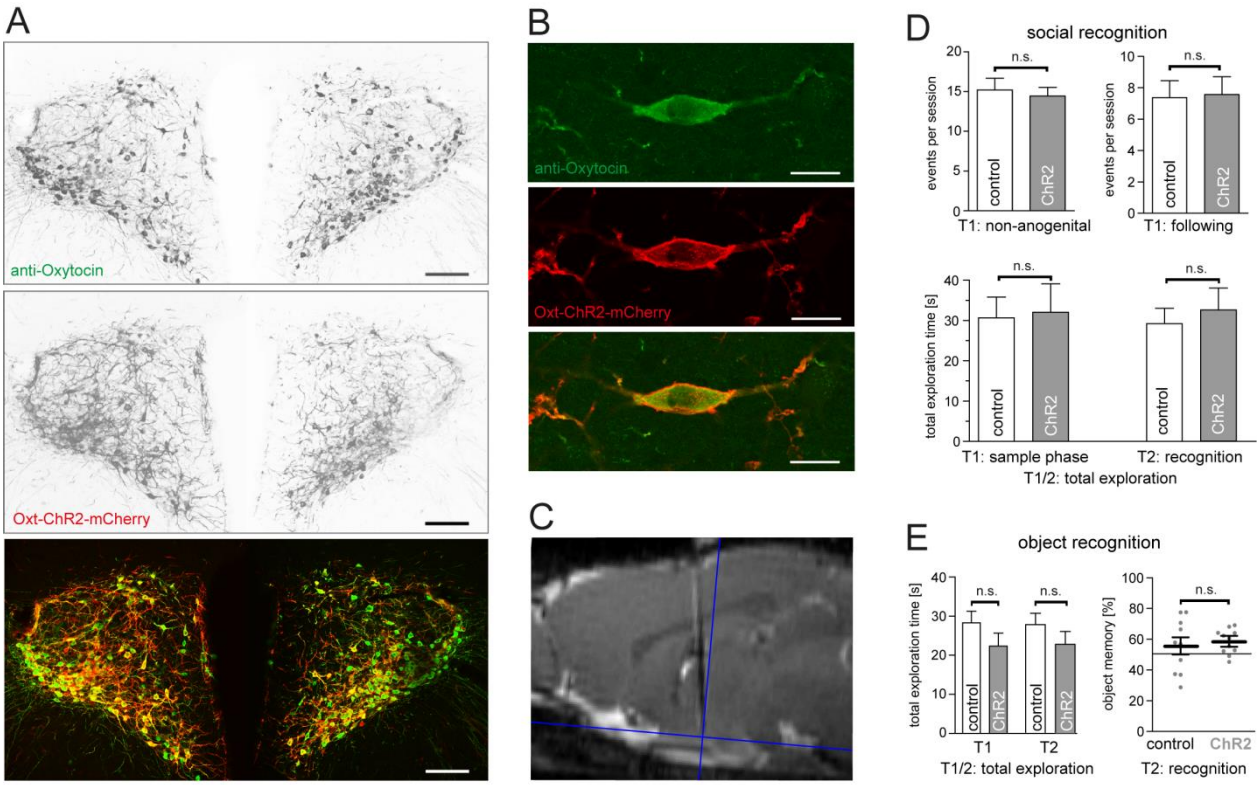

Figure S1, related to Figure 1. Evoked OXT release enhances same-sex conspecific exploration and recognition.

(A) For visualization, fluorescent images of ChR2:mCherry expression in the PVN and co-localization with OXT immunoreactivity are inverted (scale bar 150 µm). (B) Higher resolution image of ChR2:mCherry expression in the PVN and co-localization with OXT immunoreactivity (scale bar 10 µm). (C) To optogenetically evoke OXT release, a fiber optic was implanted midline above the PVNs. Placement of the fiber optic was confirmed in MRI for animals undergoing the social recognition task. (D) Top row: average number of non-anogenital or following events during the 5 min sample phase T1 of the adult rats exploring same-sex interaction partner (13 $ChR2^+$ or 11 control GFP^+ adult rats, t-test). Below: Mean total exploration time of conspecifics during the initial sample phase (T1) and subsequent recognition phase (T2) (t-test). (E) Evoked OXT release during 5 min initial object exploration did not change exploration times during the initial sample (T1) or subsequent recognition phase (T2) (left graph) and recognition of the new object in T2 (right graph: chance level at 50%) in 11 $ChR2^+$ or 10 control GFP^+ adult rats. The animals were the same as in (D) except for three animals that were removed before testing due to instable implants (t-test).

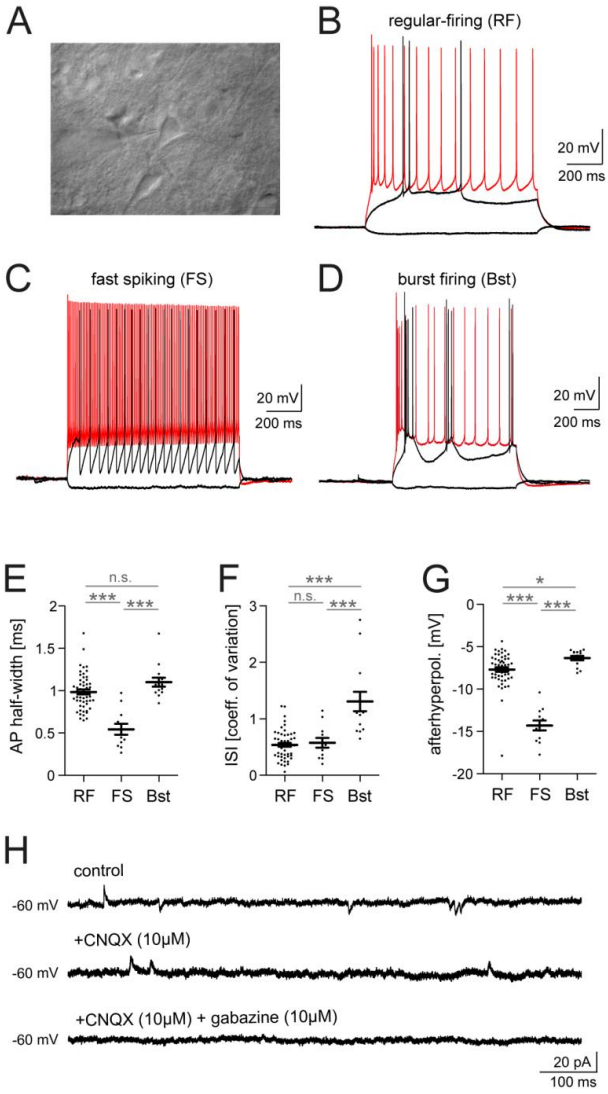

Figure S2, related to Figure 2. Firing patterns of adult AON neurons.
(A) DIC image from an adult AON slice of recorded pyramidal shaped neurons with regular firing pattern shown in (B). Recording pipet coming from left (scale bar 20 µm). (B-D) Firing response patterns following intracellular current injection in AON neurons with adapting regular-firing (B), fast-spiking (C), and burst firing pattern (D). Current steps in (B): -20, +60, +140 pA. (C): -20, +60, +360 pA. (D): -20, +60, +120 pA. (E-G) Full-width of the half-maximal action potential (E), the coefficient of variation of the inter-spike interval during 1 s positive current steps (F), and the depth of the after-hyperpolarization following action potentials during a 1 s current step (G) revealed significant differences between the sample of regular-firing (RF), fast-spiking (FS), and burst firing pattern (Bst) cells (total n=85) shown in Fig. 2A. (E-G) all ANOVA $p<0.0001$ with posttest * $p<0.05$, ***$p<0.001$. (H) Application of the AMPAR antagonist CNQX (10 µM) selectively abolished inward sPSCs while recording a regular-firing AON neuron at V_h= -60 mV in the voltage-clamp configuration. Subsequent application of the $GABA_AR$ antagonist gabazine (10 µM) abolished outward sPSCs.

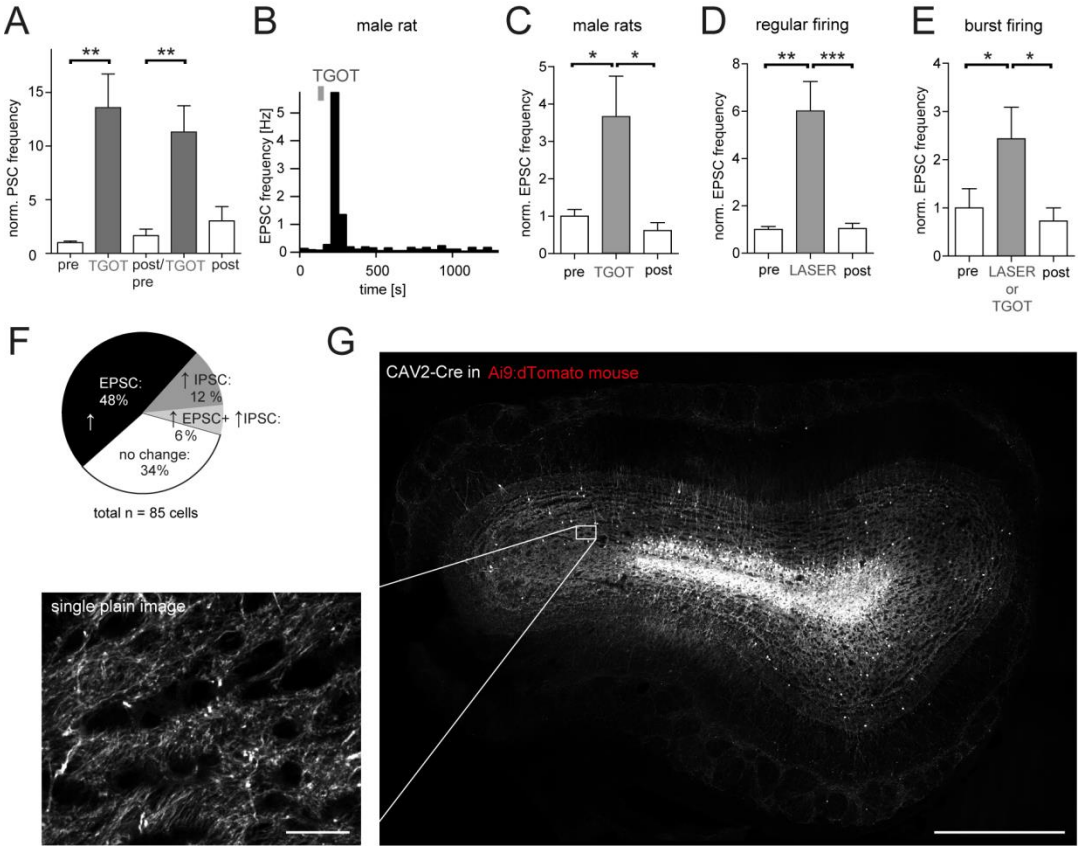

Figure S3, related to Figure 2 and 3. OXTR activation increases excitatory drive in the AON in animals of both sex.

(A) Statistical analysis of normalized sPSC rate increases following repeated TGOT application in 8 regular-firing neurons. For each cell either only sEPSC or sIPSC were analyzed. (B) Application of TGOT in a slice obtained from a male adult rat transiently increased inward sEPSCs while recording a regular-firing AON neuron at V_h= -60 mV in the voltage-clamp configuration. (C) Inward sEPSC rate reversibly increased following application of TGOT in AON neurons from male animals (n=7). (D) sEPSC rate reversibly increased in AON regular firing cells following application of laser stimulation (n=12) in rats with ChR2 expression in OXT neurons. (E) sEPSC rate reversibly increased in a set of 6 pooled AON burst firing cells following application of laser stimulation in rats with ChR2 expression in OXT neurons (n=3) or TGOT application in wild-type rats (n=3). (A, C-E) all $p<0.05$, ANOVA with post-test indicated * $p<0.05$, ** $p<0.01$, *** $p<0.001$. (F) Pooled distribution of OXT responses with an at least two-fold increase in sPSC frequency in all 85 recorded AON neurons following either evoked optogenetic OXT release or TGOT application. (G) Injection site for CAV2-Cre in the MOB of the Ai9 mouse shown in Fig. 3F (scale bar 500 µm). Inset displays higher magnification single confocal image of labeled processes in the GC layer (scale bar 30 µm).

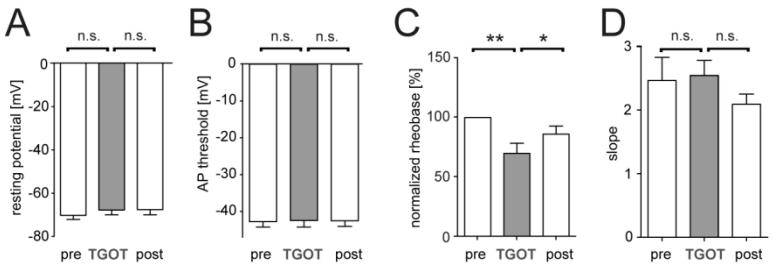

Figure S4, related to Figure 4. AON regular-firing neurons increased transiently the intrinsic excitability following OXTR activation
(A-D) Following TGOT application to 8 regular-firing AON neurons shown in Fig. 4A-C, the (A) resting membrane potential, (B) the membrane potential at which the first AP was initiated, (C) the normalized rheobase for the injected current (in percent relative to 'pre' of the same cell), (D) the slope of the f/I-curve (as shown in Fig. 4B) of each cell was examined during the same time window as the observed left shift in the input-output function in Fig. 4C. All n.s. except (C) $p<0.05$, ANOVA with post-test indicated * $p<0.05$, ** $p<0.01$.

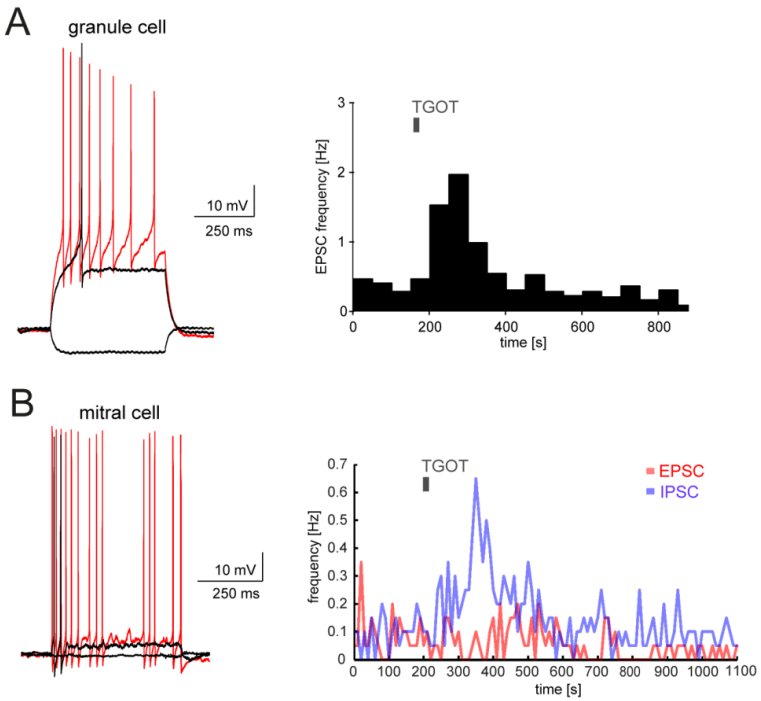

Figure S5, related to Figure 5. OXTR activation in the AON increases excitatory drive to GCs and inhibitory drive to mitral cells.
(A) Firing response of a granule cell in the MOB following intracellular current injection (left) and PSTH of the transient increase in sEPSC rate upon TGOT application (right). (B) Firing response of a mitral cell in the MOB following intracellular current injection (left) and PSTH of the transient increase in sIPSC, rate upon TGOT application (right). Note that the sEPSC rate did not change.

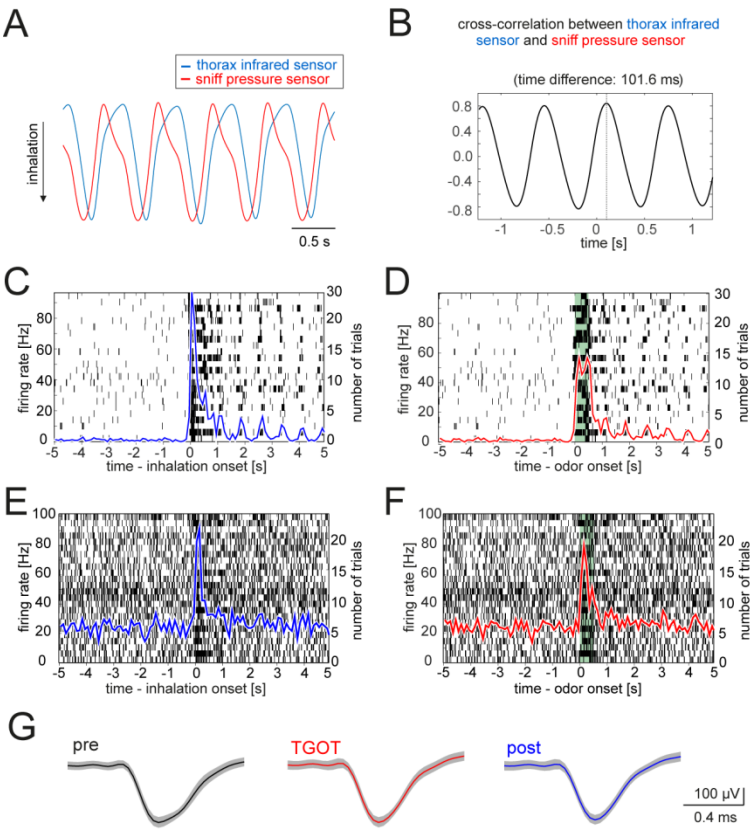

Figure S6, related to Figure 6. Influence of the sniff cycle on odor responses in M/T cells.
(A) Phase relationship of the infrared thorax distension sensor and the sniff pressure sensor measured with an intranasally implanted cannula in an adult rat under urethane anesthesia. (B) Cross-correlation between thorax distension and intranasal pressure sensor revealing a stable relationship with constant phase shift in anesthesia. (C-D) Example of M/T unit firing with low baseline firing to 0.5 s of odorant application (C) after and (D) before alignment to the sniff cycle. (E-F) Example of M/T unit firing with high baseline firing to 0.5 s of odorant application (E) after and (F) before alignment to the sniff cycle. (C-F) bin size: 100 ms. (G) Example of the spike waveform of a responsive M/T cell before, directly following TGOT application to AON and after 15 min ('post'). Data shows mean and standard deviation.

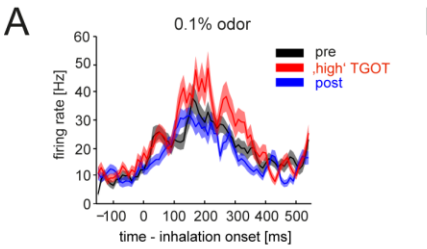

C

		pre	TGOT	post	ANOVA
time to peak of odor response [ms]	‚high' TGOT 1% odor	230.0±21.9	230.0±18.3	225.0±19.4	n.s.
	‚high' TGOT 0.1% odor	202.8±34.4	188.9±26.4	205.8±15.1	n.s.
	‚low' TGOT 1% odor	202.6±32.6	179.9±25.7	189.5±25.2	n.s.
full-with at half-maximum odor response [ms]	‚high' TGOT 1% odor	167.5±18.2	170.0±16.0	172.5±14.7	n.s.
	‚high' TGOT 0.1% odor	158.3±14.2	172.2±14.1	155.6±13.9	n.s.
	‚low' TGOT 1% odor	168.4±12.8	178.9±12.9	163.2±13.2	n.s.

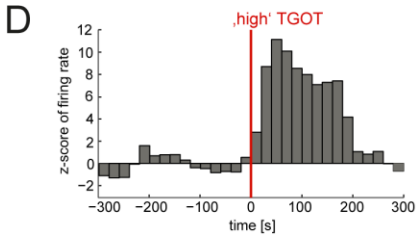

Figure S7, related to Figure 7. OXTR activation in the AON increases signal-to-noise ratios of odor responses in M/T cells and firing rates of putative GC units.
(A) Mean PSTH for 17 cell-odor-pairs in 9 putative M/T cells with 'high' TGOT in the AON. In these cells, odorants were applied at tenfold higher dilution (0.1%) than in Fig. 7. (B) TGOT increased the peak firing response to 0.1% odorants in 17 cell-odor-pairs in 9 putative M/T cells ($p<0.01$, ANOVA with post-test indicated * $p<0.05$, ANOVA). (C) The time to peak and the width at half maximum firing rate of the odor response did not change upon application of 'high' and 'low' TGOT concentrations and at different odorant dilutions (1% or 0.1%). Mean values are given for all cell-odor-pairs shown in Fig. 7 and S7A-B, respectively (all n.s., ANOVA). (D) Z-score of firing rate changes in 8 putative GC units before and directly after TGOT application in the AON.

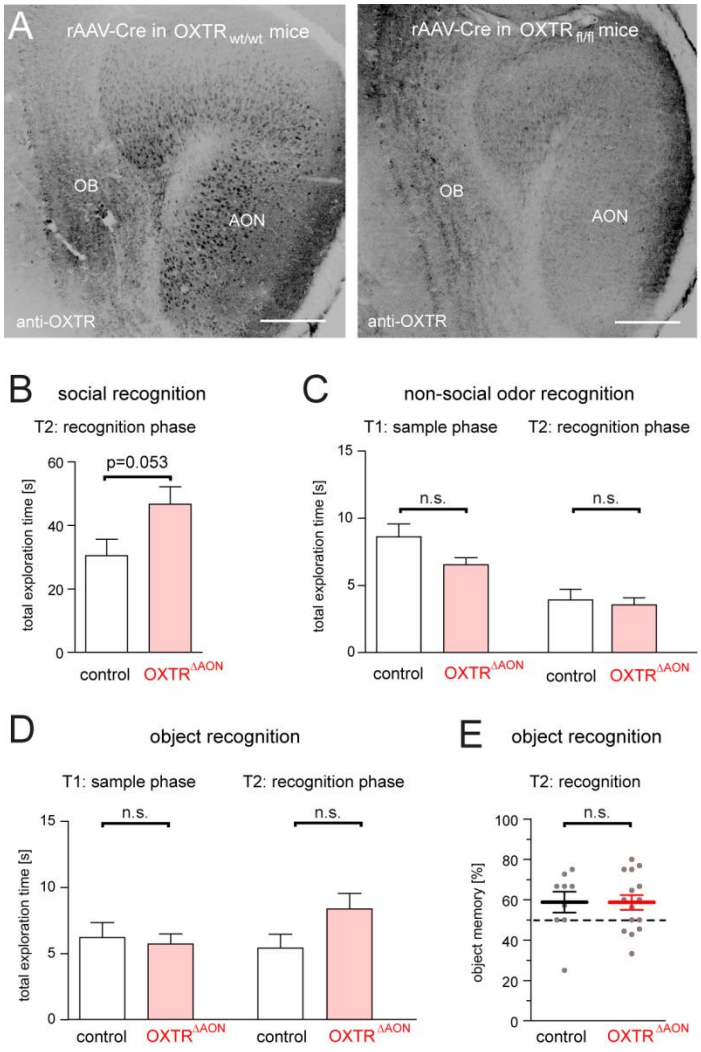

Figure S8, related to Figure 8. Impaired same-sex social recognition in mice with OXTR deletion in the AON.

(A) OXTR immunoreactivity was lost in the AON following rAAV$_{1/2}$-CBA-Cre injection in OXTR$_{fl/fl}$, but not control mice (scale bar 300 µm). For visualization, fluorescent images were inverted. (B) For the social recognition test shown in Fig. 8B-C, the mean total time spent exploring conspecifics during the recognition phase (T2) (t-test). (C) For the non-social odor recognition test shown in Fig. 8D, the mean total time spent exploring the odorants during the sample phase (T1) or recognition phase (T2) in the 13 OXTR$^{\Delta AON}$ and 8 control mice (t-test). (D) A non-social object recognition test was essentially performed as the social or odor recognition task described before: Mean total time spent exploring the objects during the sample phase (T1) or recognition phase (T2) in the 15 OXTR$^{\Delta AON}$ and 9 control mice (t-test). (E) OXTR$^{\Delta AON}$ mice did not differ in their performance in object recognition (chance level at 50%) in 15 OXTR$^{\Delta AON}$ and 9 control mice (t-test).

SUPPLEMENTAL EXPERIMENTAL PROCEDURES

Virus preparation. Recombinant (r)AAV vectors were produced with $AAV_{1/2}$ coat proteins and purified with heparin columns to a final virus concentration of $\sim 10^{16}$ genome copies/ml: $rAAV_{1/2}$-OXT-ChR2:mCherry (Knobloch et al., 2012) for selective expression of ChR2 in OXT neurons and $rAAV_{1/2}$-OXT-vGFP as the matched control virus. For Cre-dependent gene deletion in the AON, a $rAAV_{1/2}$-CBA-Cre was produced (Monory et al., 2006). For labeling of AON top-down projections a $rAAV_{1/2}$-CamKII-ChR2:mCherry was prepared (gift of K. Deisseroth). Retrograde, replication-deficient CAV2-Cre virus was prepared and obtained from Eric Kremer (IGMM Core facility, Montpellier, France).

Stereotactic surgery. Adult animals were anesthetized with isoflurane. Rats were stereotactically injected with $rAAV_{1/2}$-OXT-ChR2:mCherry (1 µl per side) bilaterally into the paraventricular nucleus of the hypothalamus (PVN) with a glass micropipette connected to a nanoinjector (MO-10, Narishige). The PVN coordinates were (in mm relative to Bregma): anterior -1.8, lateral 1.6, ventral 8.1 and a lateral angle of 8°. Optical fibers were implanted unilaterally with the following coordinates: anterior -1.8, lateral 1.2, ventral 8.3, a lateral angle of 8°, and fixed with dental acrylic. For labeling of top-down projections, $rAAV_{1/2}$-CamKII-ChR2:mCherry was injected bilaterally into the AON (1 µl per side) with the following coordinates (in mm relative to Bregma): anterior 5, lateral 1.5, ventral 4.5. After surgery, animals were returned to their home cage. For generation of $OXTR^{\Delta AON}$ mice, $rAAV_{1/2}$-CBA-Cre (0.3 µl per injection site) was injected bilaterally into the AON in $OXTR_{fl/fl}$ mice or control $OXTR_{wt/wt}$ mice (in mm relative to Bregma): anterior +3.0, lateral +-0.7, ventral -3.7, and: anterior +3.0, lateral +-1.2, ventral -3.5. For retrograde labeling of AON projections, 0.2 µl of CAV-Cre were injected unilaterally into the GC layer of the anterior half and center of the MOB of Ai9:dTomato reporter mice.

Histology. Animals were perfused with PBS 0.9% followed by 4% paraformaldehyde (PFA) and post-fixed in the same solution for 24 hrs. Serial, coronal sections (50 µm) were prepared with a vibratome and stained with primary antibodies raised against OXT (1:300; provided by Harold Gainer, NIH) (Ben-Barak et al., 1985) or OXTR (1 µg/ml, OXTR-2 antibody) (Marlin et al., 2015) overnight at 4^{o}C and visualized with A488- or Cy3-conjugated antibodies (1:1000 at room temperature for 2 hours, Jackson Immuno-Research Laboratories). Specificity of the used batch of OXTR-2 antibody was confirmed in tissue sections from global OXTR knock-out mice (Eliava et al., 2016; Marlin et al., 2015). All images were acquired with a Leica SPM5 laser scanning microscope (20x or 63x oil immersion objectives). Single confocal plains were examined for co-localization from every fifth section of the AON.

Structural MRI. Rats were anesthetized with isoflurane and 3D T2-weighted images were obtained with a 9.4 T Bruker rodent MRI to determine the position of the optical fiber in the PVN.

Behavioral analyses. *Odor and object recognition.* Short-term memory for objects and odorants was assessed with the object and the odor recognition test respectively. The design of both tests was comparable to the social recognition paradigm in mice with 5 min sample phase followed by 30 min home cage and 3 min. recognition phase. For object recognition, two identical objects were presented during the sample phase and one familiar and one new object were presented during the recognition phase. All objects and the test arena were cleaned between each test. Preliminary experiments had confirmed that the animals showed a comparable interest in the different objects. For odor recognition, odorants (amyl acetate or hexanal) were diluted in mineral oil corresponding to 1 Pa vapor pressure at room temperature applied to filter paper and hidden in stainless-steel tea balls. Again, during the sample phase two tea balls with the same odorant were presented and one familiar and one novel odorant during the recognition phase. For both recognition tests, percentage of object or odor recognition memory [time of investigation of new object/odorant B divided by (time of investigation of new object/odorant B + time of investigation of familiar object/odorant A‘)] in percent was evaluated during the recognition phase.

Odor discrimination. Mice were trained in a head-fixed operant conditioning go/no-go two odor discrimination paradigm using a protocol adapted from Slotnick and Restrepo (Slotnick and Restrepo, 2005). After attachment of a head bar, mice were allowed to recover for one week before starting water restriction to 84.3±0.7% of baseline bodyweight. Odorants were delivered with a custom-built olfactometer, with an infrared beam-break sensor (Omron Electronics, EE-SX3009-P1) to detect licking at a buttoned cannula. The training phase comprised three stages. In stage 1, licking was rewarded on a random interval schedule (0.5 – 12 s) with a drop of water (5 µl). When mice licked consistently they progressed to stage 2. Licking was only reinforced after presentation of an odorant (2.5 s,

with a variable inter-trial-interval of 10± 2 s, 120 trials). Criterion for succession to the stage 3 was an accuracy of ≥80% (proportion of earned drops to all trials) for 6 consecutive blocks of 10 trials. Using the same parameters, stage 3 introduced a second, non-reinforced odor, so mice progressively refrained from licking in the non-rewarded trials. Odorants were presented in a pseudo-randomized sequence with a maximum of three consecutive presentations of the same odorant. Accuracy was defined as N(hits)+N(correct rejections)/N(trials) per block. During the training phase, a drop was delivered automatically when no licking was recorded for 10 trials. From the 9 control and 9 $OXTR^{\Delta AON}$ mice that had been initially trained, 2 controls and 1 mutant mouse did not reach criterion (≥80% accuracy) and were therefore excluded before entering the discrimination phase. After completion of the training, the other mice were confronted with a sequence of increasingly similar pairs of mixtures of (+)- and (-)-carvone (100%/0%, 80%/20%, 60%/40%, 55%/45%, 52%/48% diluted in mineral oil so that the summed concentration of the two odorants in the mix was 1%). Each day one session was completed. Animals progressed to the next more difficult mixture independent of whether they reached criterion.

Slice Electrophysiology. Slice recordings were performed from at least 8 week-old rats. Animals were given an overdose of isoflurane and perfused intracardially with carbogenated slicing solution at 4°C containing the following (in mM): 212 sucrose, 3 KCl, 1.25 NaH_2PO_4, 26 $NaHCO_3$, 7 $MgCl_2$, 0.5 $CaCl_2$, and 10 glucose (306 mOsm, pH 7.3). Brains were incubated in cold slicing solution and cut into 350 µm sagittal slices containing the bulb and the olfactory cortex with a vibratome. For recovery, slices were incubated at 32°C for 30 min in carbogenated recording solution containing the following (in mM): 125 NaCl, 2.5 KCl, 1.25 NaH_2PO_4, 25 $NaHCO_3$, 1 $MgCl_2$, 2 $CaCl_2$, and 25 glucose (312 mOsm, pH 7.3). For recordings, the temperature of the bath solution was kept at 35°C. Whole-cell patch clamp recordings were performed with an EPC-10 amplifier (HEKA). The pipette solution contained the following (in mM): 4 KCl, 140 K-gluconate, 10 HEPES, 4 ATP-Mg, 0.3 GTP-Tris, and 10 phosphocreatine (292 mOsm, pH 7.2). For MOB granule cell recordings, Lucifer yellow (Sigma) was added to pipette solution (1mg/ml). Access resistance was <20 MΩ, and the liquid junction potential was not corrected. Resting membrane potential was determined shortly after establishing the whole-cell configuration. Membrane capacitance and resistance were determined by application of a hyperpolarizing pulse. The action potential firing pattern was determined by incremental 500 ms or 1000 ms current steps. In between steps no current was injected. Recorded neurons displayed both inward CNQX-(10 µM)-sensitive EPSCs and outward gabazine-(10 µM)-sensitive IPSCs at the same holding potential (V_h=-60 mV). Continuous sPSC recordings were analyzed with Matlab (The Mathworks) and IgorPro (Wavemetrics) with Taro Tools (Dr. Taro Ishikawa, Jikei University School of Medicine, Tokyo, Japan). For analysis of synaptic currents, events were first detected automatically, followed by a supervised analysis. Spontaneous PSC frequencies were averaged in bins of 50 seconds and time windows of 100 seconds were taken from the whole recording before, during and following stimulation to compare different conditions. For the cell-type characterization shown in Fig. S2E-G, the following properties were determined. The full-width of the half-maximal action potential and the maximal depth of the after-hyperpolarization following action potentials (measured relative to the onset of the fast rising phase of the action potential) were both measured during a 1 s positive current step at rheobase of the respective cell. The inter-spike interval (ISI) was determined from all spikes in the first three incremental 1 s current steps following rheobase (excluding the first action potential in each current step). The coefficient of variation was determined by dividing the standard deviation of the ISI distribution by the mean of the ISI.

OXTR agonist application. In voltage-clamp mode (V_h=-60mV), the baseline was recorded for 200 seconds. For local application of oxytocin receptor agonist, positive pressure (1-2 psig) was applied to a glass pipette (2-3 µm diameter) filled with the highly selective OXTR agonist [Thr4,Gly7]-oxytocin (TGOT; 1 µM) in ACSF. To avoid tachyphylaxis, the agonist was applied at intervals of 20 minutes, resulting in repeatability of the response (Huber et al., 2005). For experiments requiring blockade of fast sodium channels, TTX (1 µM) was added to the recording solution.

Optogenetic OXT stimulation. For optogenetic OXT stimulation experiments, slice preparations were prepared from animals that were injected with $rAAV_{1/2}$-OXT-ChR2:mCherry into the PVN. In voltage-clamp mode (V_h=-60 mV), the baseline of synaptic currents was recorded for at least 200 seconds. The same stimulation protocol used for behavioral experiments (5 ms pulses at 30 Hz for 2-20s) was then applied to an optic fiber attached to a TTL triggered 473 nm-DPSS-Laser (Shanghai Laser & Optics).

AON recordings. Recordings were performed in area pars principalis of the anterior olfactory nucleus (Brunjes et al., 2005). For the analysis of intrinsic excitability, TGOT was applied to AON neurons in presence of CNQX (10 µM), gabazine (10 µM) and D-AP5 (50 µM). Incremental current steps were applied to the cell throughout the recording and the recorded f-I curves were fitted by applying a linear regression model and the point of intercept with the x-axis was determined as rheobase.

MOB recordings. GCs were identified by morphology and location in the GC layer. Mitral cells were targeted in the mitral cell layer and based on their large triangular cell bodies in DIC. Both cell types were recorded in voltage-clamp at their resting potential. For optogenetic stimulation of AON top-down projections, GCs were recorded and stimulated with blue laser pulses (2 ms) at different frequencies. Decay of both evoked and spontaneous EPSC events was analyzed by exponential fits. The data for the spontaneous events were classified as slow, if their decay time exceeded 8 ms, and they were classified as fast if their decay time was below 6 ms.

Statistical analyses. Except where otherwise indicated data was normally distributed (Kolmogorov-Smirnov test) and the compared groups did not significantly differ in their variance (F-test). Unpaired two sided Student t-tests were used if comparisons were made across cells or animals and paired two-sided t-tests for with cell drug effects (p-values >0.05 indicated as n.s.). ANOVA with Bonferroni post-tests were used throughout at the indicated significance levels. For ANOVA, p-values >0.05 are indicated as n.s. Repeated-measure ANOVA was applied if effects in the same cells were examined.

SUPPLEMENTAL REFERENCES

Ben-Barak, Y., Russell, J.T., Whitnall, M.H., Ozato, K., and Gainer, H. (1985). Neurophysin in the hypothalamo-neurohypophysial system. I. Production and characterization of monoclonal antibodies. The Journal of neuroscience : the official journal of the Society for Neuroscience *5*, 81-97.

Brunjes, P.C., Illig, K.R., and Meyer, E.A. (2005). A field guide to the anterior olfactory nucleus (cortex). Brain research Brain research reviews *50*, 305-335.

Eliava, M., Melchior, M., Knobloch-Bollmann, H.S., Wahis J., d.S.G., Tang, Y., Ciobanu, A.C., Triana del Rio, R., Roth, L.C., Althammer, F., Chavant, V., *et al.* (2016). A new population of parvocellular oxytocin neurons controlling magnocellular neuron activity and inflammatory pain processing. Neuron *in press*.

Huber, D., Veinante, P., and Stoop, R. (2005). Vasopressin and oxytocin excite distinct neuronal populations in the central amygdala. Science *308*, 245-248.

Knobloch, H.S., Charlet, A., Hoffmann, L.C., Eliava, M., Khrulev, S., Cetin, A.H., Osten, P., Schwarz, M.K., Seeburg, P.H., Stoop, R., *et al.* (2012). Evoked axonal oxytocin release in the central amygdala attenuates fear response. Neuron *73*, 553-566.

Marlin, B.J., Mitre, M., D'Amour J, A., Chao, M.V., and Froemke, R.C. (2015). Oxytocin enables maternal behaviour by balancing cortical inhibition. Nature *520*, 499-504.

Monory, K., Massa, F., Egertova, M., Eder, M., Blaudzun, H., Westenbroek, R., Kelsch, W., Jacob, W., Marsch, R., Ekker, M., *et al.* (2006). The endocannabinoid system controls key epileptogenic circuits in the hippocampus. Neuron *51*, 455-466.

Slotnick, B., and Restrepo, D. (2005). Olfactometry with mice. Current protocols in neuroscience / editorial board, Jacqueline N Crawley [et al] *Chapter 8*, Unit 8 20.